NUMERICAL INVESTIGATIONS OF THE FLOWS AROUND VARIOUS CRUCIFORM WING-BODY CONFIGURATIONS AT MACH NUMBERS FROM 2. TO 10. AND ARBITRARY ANGLES OF ATTACK USING SYCHEV'S THEORY

N.V.Voevodenko
Central Aerohydrodynamic Institute (TsAGI), Zhukovsky, Moscow Region, Russia

Abstract

Supersonic flows over slender bodies at various angles of attack have been investigated using numerical method based on Sychev's generalization of hypersonic small-disturbance theory and Godunov's method. The theoretical and numerical investigations have been performed to determine the method applicability range. This investigations have shown that the method under consideration and the program based on it are applicable to a great variety of configurations, and that the applicability range is much greater than it was assumed by basic theory. The studies have been conducted to determine the possibility of this method to calculate the flow parameters and aerodynamic characteristics of various configurations, such as: 1) bodies of revolution with various generatrix, 2) cruciform wing-body, 3) cruciform wing-body-canards. Comparison of numerical results with experimental data indicate that this method can be reliably applied to such practical configurations.

Introduction

The problem of the flows calculations for slender bodies at high supersonic velocities and arbitrary angles of attack is considered in the frame of hypersonic small disturbance theory (flat sections law) generalized by V.V. Sychev on the case of arbitrary angles of attack (Sychev's theory[1]). The calculation of 3-D flows around bodies at high angles of attack and supersonic speeds is rather complex and difficult problem for the usual 3-D numerical methods. The approximate fast methods (for example, based on Newton's theory, or conical-shock-expansion theory, or linear theory and so on) permit us to consider the narrow classes of geometry only (usually, these are the slender bodies close to axisymmetric).

Sychev's theory in combination with numerical method makes it possible to solve the above mentioned problem for wide class of airframes rapidly and reliably.

A number of papers, for example[2,3] were devoted to the investigations of the Sychev's theory applicability range and to the use of Sychev's similarity parameters, which follow from Sychev's theory, for the experimental data analysis.

The numerical method and the programme package (NINA), based on Sychev's generalization of hypersonic small disturbance theory and Godunov's method, are presented by this paper.

A theoretical investigation have been done to determine the applicability region of this method. Such investigations indicate that this method is applicable to a wide class of airplane and airspace configurations.

This method is used for the studies of the flows around variety of airframes at supersonic/ hypersonic speeds and at wide range of angles of attack.

An investigation has been conducted to determine the effectiveness of this method in predicting the aerodynamic characteristics and pressure distributions over various cruciform wing-body configurations at Mach numbers from 1.5 to 4.63. The numerical results are compared with experimental data.

Theoretical consideration.

1. We consider the ideal gas supersonic flow over slender body at α – angle of attack. d – denotes the maximum body cross-section dimension, ℓ – the length of the body.

Following[1] we suppose that

$$\delta = \frac{d}{\ell} \ll 1, \quad M_\infty \sin\alpha \gg 1; \quad M_\infty \delta \gtrsim 1 \qquad (1.1)$$

When suppositions (1.1) are valid, the original problem is equivalent to the flat unsteady gas motion problem. Such 2-D unsteady motion is initiated by the extension of the flat piston. The piston form is determined by the form of the body cross sections.

2-D unsteady ideal gas motion is described by the following set of equations:

$$\frac{\partial \bar{\sigma}}{\partial t}+\frac{\partial \bar{b}}{\partial y}+\frac{\partial \bar{c}}{\partial z}=0$$

$$\bar{\sigma}=\begin{pmatrix}\rho\\ \rho V\\ \rho W\\ e\end{pmatrix};\quad \bar{b}=\begin{pmatrix}\rho V\\ p+\rho V^2\\ \rho VW\\ (e+p)V\end{pmatrix};\quad \bar{c}=\begin{pmatrix}\rho W\\ \rho VW\\ p+\rho W^2\\ (e+p)W\end{pmatrix};\quad (1.2)$$

$$e=\rho\left(\varepsilon+\frac{V^2+W^2}{2}\right)$$

As it was demonstrated by paper[1], in this case the equations and boundary conditions depend on two parameters

$$K_1=\delta\,\mathrm{ctg}\,\alpha,\quad K_2=M_\infty\sin\alpha \qquad (1.3)$$

only.

If angle of attack is small, the parameter K_1 is not significant and the solution depends on the parameter K_2 only. So, Sychev's theory[1] transforms into Hayes's hypersonic small disturbance theory[4].

2. But the restrictions (1.1) of the theory[1] are too strong. It was shown by paper[7] that the requirement $M_\infty\sin\alpha\gg 1$ can be substituted by $M_\infty\sin\alpha>1$. So, the velocity component normal to the body axis can be any supersonic. But theory[1] is correct even at $M_\infty\sin\alpha<1$, if $M_\infty\gg 1$, $M_\infty\delta=O(\delta)$. In this case $\alpha=O(\delta)$ and theory[1] transforms into theory[4].

The requirement $\delta=d\ell^{-1}\ll 1$ is too strong also. This requirement restricts the class of the bodies under consideration by the configurations which all cross-section sizes are small in comparison with longitudinal one.

In paper[2] it was demonstrated that the Sychev's similarity parameters (1.3) are correct for the small-swept wings, elliptical cones and for rectangular wing even.

Using NINA-package we have investigated the Sychev's theory applicability region. We have considered the delta wings of a great variety of sweep and compared the NINA results with the 3-D numerical methods results and exact analytical solutions. The results are obtained for $M_\infty=2\div 10$; $\alpha=0\div 60°$; $\varphi=0\div 70°$.

In dependence on three parameters: M_∞, α, φ, three various regimes of the flow over delta wing can be realized: 1) the flow with bow shock wave attached to the leading edges, 2) the flow with bow shock wave attached to the wing top but coming off the leading edges, 3) the flow with shock wave coming off the leading edges and off the wing top.

Let us consider the regimes 1) and 2) only.

The results at regime 1) have been compared with results[8]. The investigations have been conducted for $M_\infty=2.5\div 10$; $\alpha=0\div 40°$ and $\varphi=30°\div 70°$. C_p distributions over wing span for a number of typical regimes are demonstrated by fig. 1. Curves 1 correspond to $M_\infty=10$, $\alpha=40°$, $\varphi=60°$; curves 2 – $M_\infty=5$, $\alpha=30°$, $\varphi=60°$, curves 3 – $M_\infty=10$, $\alpha=20°$, $\varphi=45°$, curves 4 – $M_\infty=3.5$, $\alpha=20°$, $\varphi=45°$. Solid lines are NINA's results, touch lines are the results of the characteristics method[8]. ψ is the angle between longitudinal axis and the ray from the wing top to the current point on the wing surface.

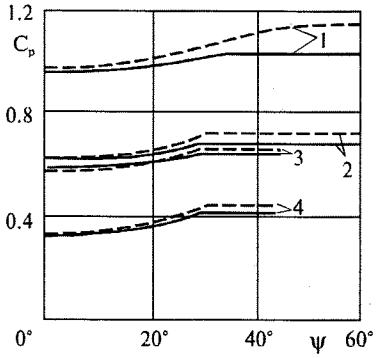

FIGURE 1

Fig. 1 demonstrates that the greatest divergence of the two methods results is located at the neighborhood of the leading edge.

When the shock wave is attached the flow on the compression side about leading edge is analogous to the flow behind the oblique shock-wave.

The velocity component in the flat section, normal to the wind axis, is $U_n=U_\infty\sin\alpha$. And the velocity component in the plane of wing is $U_t=U_\infty\cos\alpha$ (fig. 2). The velocity component, normal to the leading edge and lying in the wing plane, is $U_1=U_\infty\cos\alpha\sin\varphi$. Mach number in front of the shock wave is $M=M_\infty\sqrt{\sin^2\alpha+\cos^2\alpha\cdot\sin^2\varphi}$ and the wedge angle is θ: $\mathrm{tg}\,\theta=\mathrm{tg}\,\alpha\cdot\sin^{-1}\varphi$, (fig. 2). So, the flow over leading edge can be considered as analogous to the 2-D flow after oblique flat shock wave in the plane, normal to the leading

edge. In this case, we have the exact analytical solution in the region over leading edge.

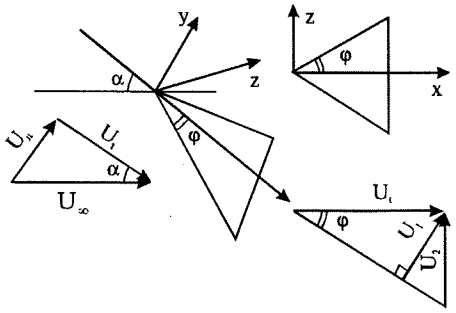

FIGURE 2

Theory[1] deals with unsteady 2-D flow in the plane, normal to the wing symmetry axis. So, in the theory[1] approach, the flow run into the leading edge with velocity $U_2 = U_\infty \cos\alpha \operatorname{tg}\varphi$. Than the flow after oblique shock wave has another Mach number and wedge angle:

$$M = M_\infty \sqrt{\sin^2\alpha + \cos^2\alpha \operatorname{tg}^2\varphi}; \quad \operatorname{tg}\theta = \frac{\operatorname{tg}\alpha}{\operatorname{tg}\varphi}.$$

So, the error of theory[1] in comparison with exact solution around leading edge can be determined analytically, and as it is the greatest one on the compression side of the wing (as shown by fig. 1), this error determines the whole error of theory[1] on the wing compression side.

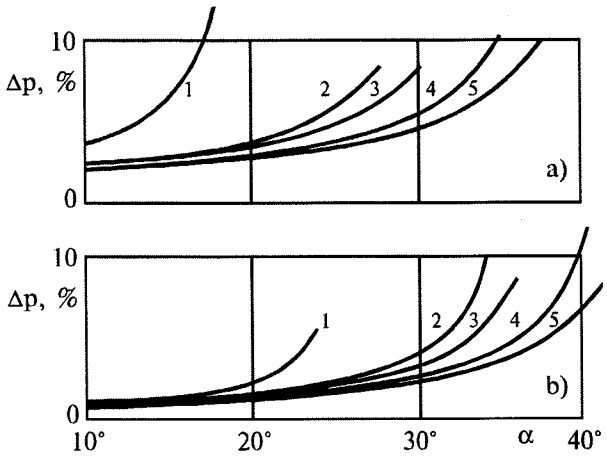

FIGURE 3

The dependence of the theory[1] error $\Delta p = (p_1 - p)\cdot p^{-1}$ (where p_1 is the pressure obtained by theory[1], p – the exact solution) on the angle of attack α at Mach number $M_\infty = 5$ is shown by fig. 3,a and at $M_\infty = 10$ – by fig. 3,b. The number of curve corresponds to each half-angle at the wing top: 1 – φ=30°, 2 – φ=45°, 3 – φ=50°, 4 – φ=60°, 5 – φ=70°. Figures 3,a and 3,b show that usually the error of theory[1] don't exceed 10%. In the range under consideration the error is biggest at M_∞=3, α=30°, φ=70° and is of value 15%.

The fact that the theory[1] error decreases with the angle φ increase is absolutely unexpected. It seems as this result is in the contradiction with one of basic assumptions of theory[1]: $\delta = d\ell^{-1} \ll 1$. But let us remind about the fact that the general parameter which determines the theory[1] error is the disturbed layer thickness. The disturbed layer thickness over leading edge decreases with φ increase because of Mach number of the flow running into leading edge increases.

Let us consider the regime 2), when the shock wave is attached to the wing top, but coming off the leading edges of delta wing. The results of such regimes calculations by NINA-programme have been compared with the results of 3-D second order numerical method[9]. The investigations have been conducted in the range: M_∞=4–10, α=30°–60°, φ=10°–20°. Fig. 4 shows the pressure p/p_∞ distribution on the compression side of the wing at M_∞=6, α=40°. Curve 1 corresponds to φ=10°, 2 – φ=15°, 3 – φ=20°. Solid lines are NINA's results and touched lines are the results of paper[9]. Like regime 1), in this case the greatest error is located over leading edge.

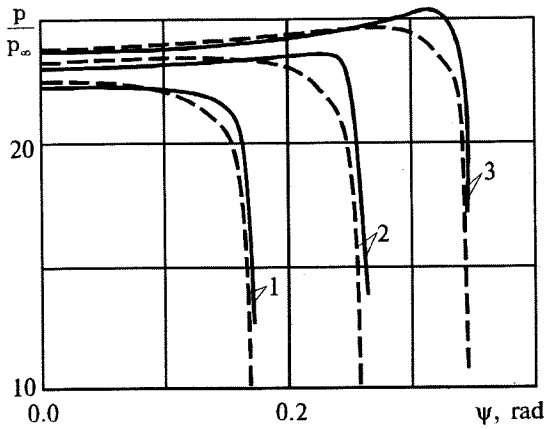

FIGURE 4

Calculation results show that the character of the theory[1] error dependence on Mach number, angle of attack and half-angle at wing top is keeping the same as for regime 1) and 2).

So, as it was shown by numerical investigations and by analytical consideration Sychev's

theory[1] is applicable not only to the bodies close to axisymmetric one, but to the bodies with wings of various form up to small-swept and rectangular wings.

3. The small disturbance theory, generalized by paper[1] on the case of high angle of attack, is correct for slender bodies with accuracy $\sim O(\delta^2)$. The span to length parameter λ can be used as parameter δ for wings. The analysis of the previous results and experimental data[2] shows that similarity parameters and the solutions obtained by theory[1] are applicable up to $\lambda\sim 1$. Moreover, when $\lambda\to\infty$ (flat problem) the solution obtained by theory[1] has an acceptable accuracy.

Let us consider the simple example of the flow over wedge with angle $\alpha\sim 1$ at the top. We consider the regime when the shock wave is attached to the wedge top. X-axis is directed along the inclined wedge surface. In the frame of flat section law this problem transforms to the 1-D problem of shock wave motion, so

$$p' = \frac{2}{æ+1}\cdot\frac{1}{\left(1-\rho/\rho_\infty\right)^2} - \frac{æ-1}{æ+1}\frac{1}{æ M_n^2},$$

$$p' = \frac{p}{\rho_\infty U_\infty^2 \sin^2\alpha}, \quad \frac{\rho}{\rho_\infty} = \frac{æ-1}{æ+1} + \frac{2}{(æ+1)M_n^2}, \qquad (3.1)$$

$$M_n = M_\infty \sin\alpha$$

If parameter ε is small, $\varepsilon=\rho_\infty/\rho\ll 1$, we can obtain using (3.1) that the difference between solution (3.1) and exact solution is about $O(\varepsilon^2)$.

Let expand in series:

$$p' = \frac{2}{æ+1}(1+2\varepsilon) + O\left(\varepsilon^2\right) \qquad (3.2)$$

and compare with exact solution:

$$p' = \frac{2}{æ+1}\frac{\sin^2\beta}{\sin^2\alpha} - \frac{æ-1}{æ+1}\cdot\frac{1}{æ M_n^2}, \qquad (3.3)$$

$$\beta = \alpha + \varepsilon\,\mathrm{tg}\,\alpha + O\left(\varepsilon^2\right)$$

After corresponding substitutions and series expansion of (3.3) we obtain (3.2) again with accuracy $\sim O(\varepsilon^2)$.

So, when we use theory[1] for calculations on the compression side of any-swept wings ($\lambda\sim 1$), a small parameter should be treated as the angle between shock-wave and wing surface. So, when $\lambda=O(1)$, it is necessary to require the parameter ε to be small, $\rho/\rho_\infty=\varepsilon\ll 1$.

4. Now we consider the flow over a wing surface which has a small deformation and a sharp leading edges at the regime with shock-wave attached to the edges. Let $\varepsilon\ll 1$, $n_x\sim\varepsilon$, $n_y\sim 1$, $n_z\sim\varepsilon$, where n_x, n_y, n_z are the components of a unit vector normal to the wing surface in a coordinate system shown by fig. 2.

If we limit the equation members order by $O(\varepsilon^2)$, then, as it is shown in paper[10], the equations and boundary conditions which describe the problem, are splitting up. After substitution of $t=xL/U_\infty\cos\alpha$ instead of X, the equations and boundary conditions are transformed into 1-D unsteady one.

Note, that this equations solution depends on the same three parameters $K_1=\lambda\,\mathrm{ctg}\,\alpha$, $K_2=M_\infty\sin\alpha$, æ. Note also, that this equations don't include the derivatives by Z (so, Z is the parameter only). So, theory[1] transforms into straps theory at $\lambda=O(1)$, like small disturbance theory[4].

It can be shown that theory[1] is also applicable to the flows over more complex airframes such as a number of slender bodies with parallel longitudinal axis, or slightly deformed wings (so that $n_x=O(\varepsilon)$, $n_y=O(1)$, $n_z=O(1)$).

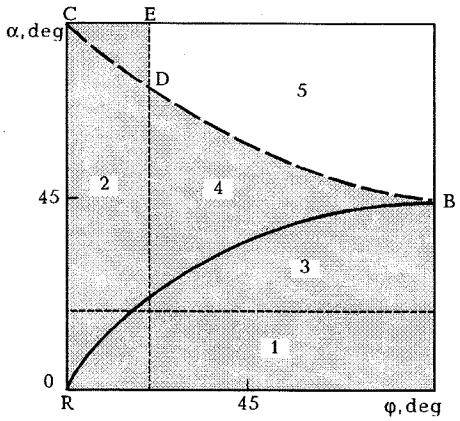

FIGURE 5

So, theory[1] and the programme based on it are able to calculate the flows over much more wide class of configurations then it mentioned by paper[1]. Fig. 5 shows schematically the applicability region of small disturbance theory (hatched region). The touched lines indicate the

boundaries which can be determined only approximately.

Region 1 corresponds to the small angles of attack, so the Hayes's theory[4] is applicable in this region. At high φ theory[4] transforms into straps theory.

Region 2 corresponds to the initial restrictions introduced in paper[1] (bodies which all cross-section dimensions are small in comparison with longitudinal one).

The region located under AB-curve corresponds to the flows with shock-wave attached to the leading edges. As it was shown above in this paper, theory[1] is applicable in region 3 with the same accuracy $O(\delta^2)$, and at high φ theory[1] transforms into straps theory.

Curve BC can be determined only approximately. Region 5 is located above curve BC and corresponds to the flows with shock-wave coming off the wing top (regime 3). In region 5 the small disturbance theory is not applicable with the exception of small region CDE, which is the case of very thing bodies in all cross-section dimensions.

For arbitrary swept wings in region 4, where shock-wave is coming off the leading edges, but attached to the wing top, we can't obtain the strict proof of the small disturbance theory applicability. If the angle at wing top is high, this theory is not correct around leading edges, but it is correct at the central part of the flow. In this case the disturbed region should be divided into two parts: 1) entropy layer which spreads far downstream from the subsonic regions over leading edges; 2) region where small disturbance theory is applicable. In the entropy layer all flow parameters besides pressure change considerably. But pressure stays almost constant. So, in region 4 it is possible to use the small disturbance theory for calculations of pressure and total aerodynamic characteristics.

Results

Programme NINA based on theory[1] is able to calculate the various classes of airframes such as:

- isolated body,
- body-wing configuration,
- body-wing-canard configuration,
- body-wing-stabilizer-tail configuration,
- all above mentioned configurations with engine,
- two bodies configuration.

It can be quickly adjusted for many types of shapes by creating a corresponding file of geometry. But this work has been done to investigate the ability of this method to calculate the flow and aerodynamic characteristics of various cruciform body-wing-tail configurations.

Bodies of revolution

The first stage of such investigation was done for a series of four bodies of revolution at Mach numbers from 1.6 to 4.63 for angles of attack from 0 to 60°. Four bodies representing various amounts of nose bluntness, midsection slope, and afterbody closure are presented by fig. 6; each has a circular cross section.

B1

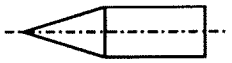

Cone cylinder

$$r/\ell = 0.16667 \cdot x/\ell \quad (0 < x/\ell < 0.45)$$
$$r/\ell = 0.075 \quad (0.45 < x/\ell < 1)$$

B2

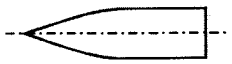

Circular-arc-cylinder

$$r/\ell = \sqrt{(1.3125)^2 + (x/\ell)(0.9 - x/\ell)} - 1.3125 \quad (0 < x/\ell < 0.45)$$
$$r/\ell = 0.075 \quad (0.45 < x/\ell < 1)$$

B3

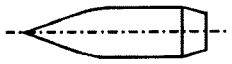

Circular-arc-cylinder-boattail

$$r/\ell = \sqrt{(1.3125)^2 + (x/\ell)(0.9 - x/\ell)} - 1.3125 \quad (0 < x/\ell < 0.45)$$
$$r/\ell = 0.075 \quad (0.45 < x/\ell < 0.9)$$
$$r/\ell = 0.075 - 0.105(x/\ell - 0.9) \quad (0.9 < x/\ell < 1)$$

B4

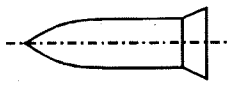

Circular-arc-cylinder-flare

$$r/\ell = \sqrt{(1.3125)^2 + (x/\ell)(0.9 - x/\ell)} - 1.3125 \quad (0 < x/\ell < 0.45)$$
$$r/\ell = 0.075 \quad (0.45 < x/\ell < 0.9)$$
$$r/\ell = 0.075 + 0.105(x/\ell - 0.9) \quad (0.9 < x/\ell < 1)$$

FIGURE 6

Calculation results have been compared with experimental data obtained in the Langley

Unitary Plan wind tunnel paper[11]. The results of this investigation are shown by figures 7-10.

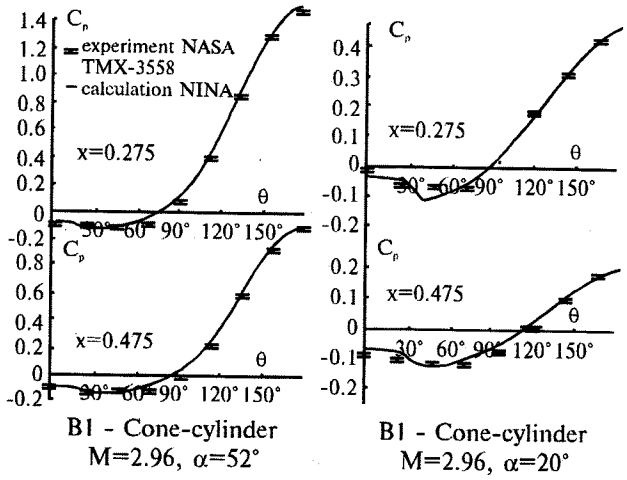

FIGURE 7

C_p distribution over two typical cross sections X=0.275, 0.475 for con-cylinder (B1) at Mach number 2.96 and two angles of attack α=20°, 52° are presented on fig. 7. Note that the results coincidence is acceptable not only on the compression side of the body but on the leeward side too.

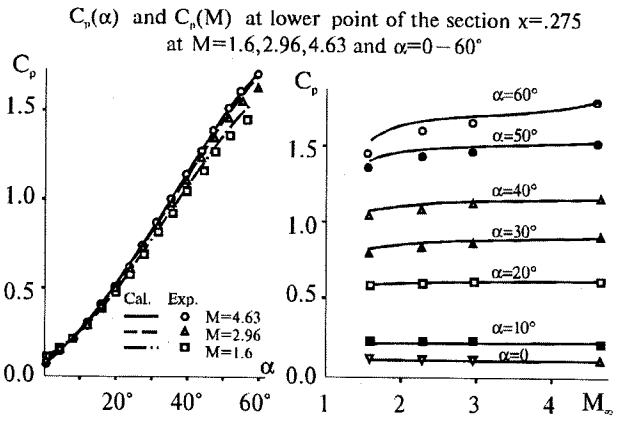

FIGURE 8

Fig. 8 demonstrates the results behavior in the whole range of Mach numbers and angles of attack. C_p at a lower point of the section X=0.275 is taken for all regimes. The largest difference between NINA-results and experimental data is obtained at M_∞=1.6 and α=60°. But even in this case the results difference is not more then 8%.

C_p for B1 at lower point of the section in the various cross sections X=0.275, 0475, 0.675, 0. 875 is shown on the left part of fig. 9 at M_∞=2.3. Right part of fig. 9 demonstrates the results coincidence along body axis (C_p is taken at a lower point of cross-section) for M_∞=2.96.

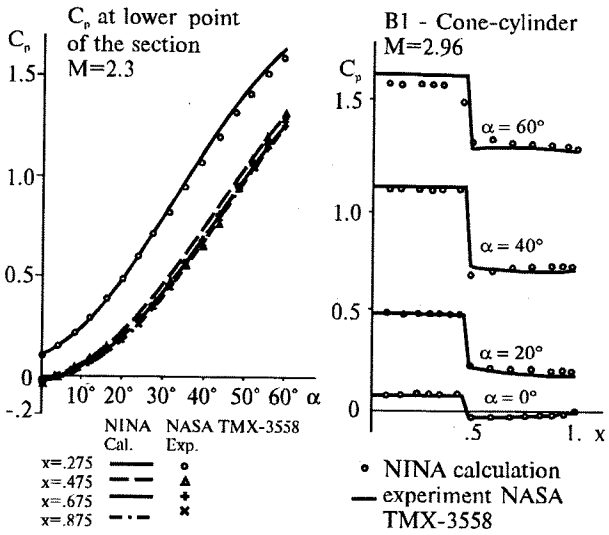

FIGURE 9

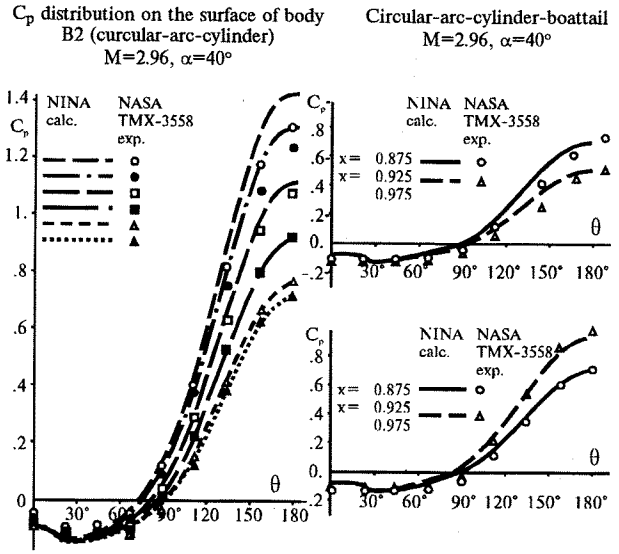

FIGURE 10

Fig. 10 presents the results for circular arc-cylinder (body B2), for circular arc-cylinder-boattail (body B3), and for circular arc-cylinder-flare (body B4) at one typical regime M_∞=2.96, α=40°. C_p dependence on θ (θ is circumferential angle, measured clockwise looking aft) in various cross-sections at M_∞=2.96, α=40° is shown. The largest difference 8% is observed at lower point of the section X=0.075. Fig. 10 demonstrates that the numerical method based on theory[1] can be successfully applied to the calculations of the bodies of revolution with various generatrix.

The investigation, which have been conducted, shows that the method under consideration is applicable in a wide range of Mach numbers and angles of attack to the various body forms, various amount of nose bluntness, midsection slope, and afterbody closure.

Body+wings of various planform

The next stage is the investigation of this method applicability to the bodies with wings of various planeform. The planeforms include a family of delta wings, rectangular wings, and cranked-tip wings. Sketches of the models are shown in fig.11.

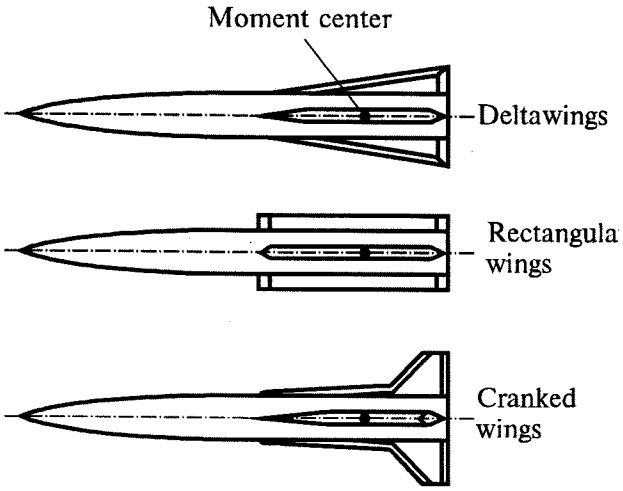

Sketch of tested wing-body configurations NASA TMX-1839

FIGURE 11

Calculation results have been compared with the experimental data obtained in the Langley Unitary Plan wind tunnel and presented in paper[12]. The investigation have been done at Mach numbers from 2.3 to 4.63 and α=0-40°. Present investigation was undertaken in order to determine the possibilities of this method to obtain the total characteristics for body with various wings. The model were investigated at two roll angles: φ=0 (scheme +) and φ=45° (scheme X).

Numerical results and experimental data are shown by figures 12-16. The results for body with tree delta wings (large, mid and small) at roll angle φ=0 (scheme +) and isolated body are demonstrated on fig. 12. Experimental data[12] are obtained in the range of α=0−20°. But numerical investigations have been done at α=0−40°.

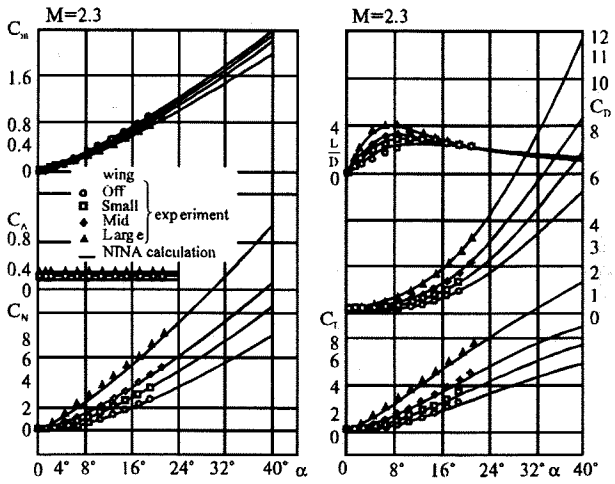

Effect of delta wing on the longetudinal aerodynamic characteristics, φ = 0° (scheme +)

FIGURE 12

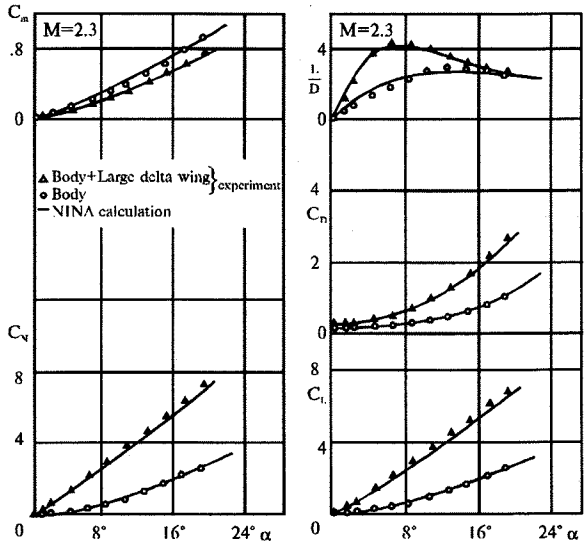

Effect of delta wing on the longetudinal aerodynamic characteristics, φ=45° (scheme X)

FIGURE 13

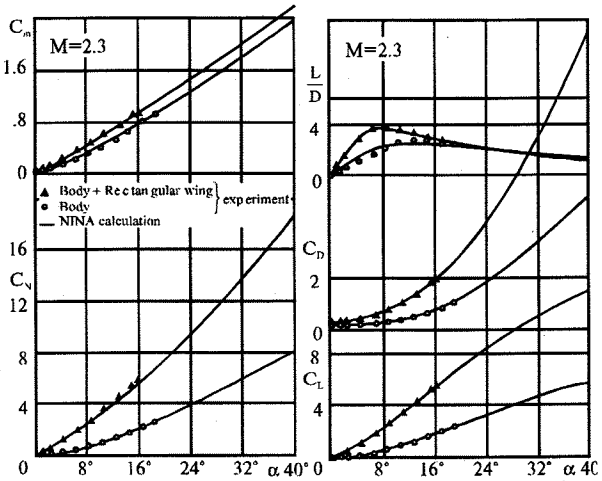

Effect of rectangular wing on the longetudinal aerodynamic characteristics, φ=0° (scheme +)

FIGURE 14

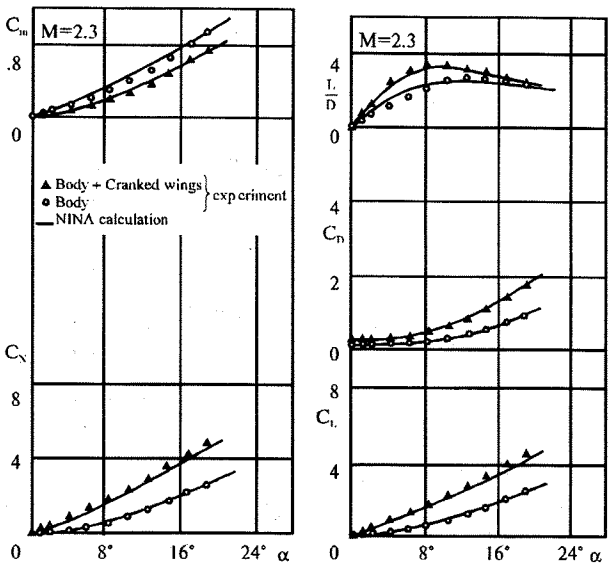

Effect of cranked wings on the longetudinal aerodynamic characteristics, φ=45° (scheme X)

FIGURE 15

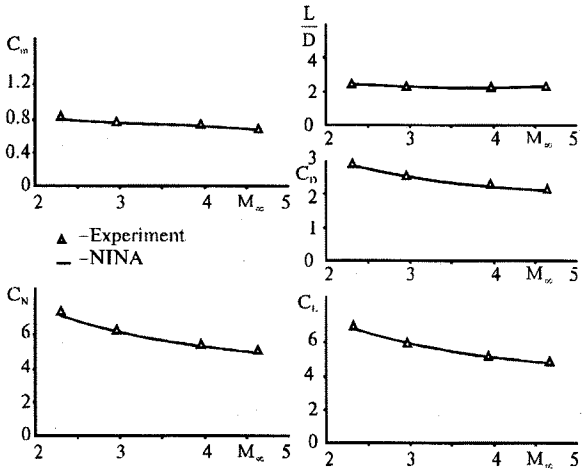

Body + large delta wings, φ= 0 (scheme +) α = 20°

FIGURE 16

Fig.13 presents the results for body with large delta wing at roll angle φ=45° (scheme X).

Effect of rectangular wing at φ=0 (scheme +) is shown by fig.14. Results for cranked wings at φ=45° (scheme X) are presented on fig.15.

Aerodynamic characteristics of body+large delta wing at α=0 and α=20° in the Mach number range M_∞=2.3-4.63 are presented on fig.16.

The above investigations demonstrate that the numerical method under consideration can be reliable applied to the total aerodynamic characteristics calculation for the configurations of body+wing of various planeform.

Body+wing. Pressure distribution

An investigation has been conducted to determine the possibility of the method in predicting the pressure distributions over wing-body configuration. Numerical pressure coefficients are compared with experimental values obtained on a delta planeform wing-body model in the Langley Unitary Plane wind tunnel[13] at Mach numbers from 2.30 to 4.63 and angles of attack to 11°.

A drawing of the model is presented in fig.17.

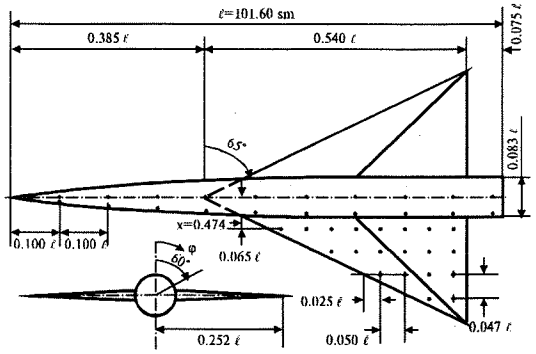

Sketch of model showing location of pressure orifices

FIGURE 17

Comparison of the body experimental data with NINA's calculation at M_∞=4.63 and α=6.2°, 10.4° is presented by fig. 18,a and 18,b, where is circumferencial angle, measured as shown by fig.17. Pressure coefficients over wing distribution is shown by fig. 19,a and 19,b.

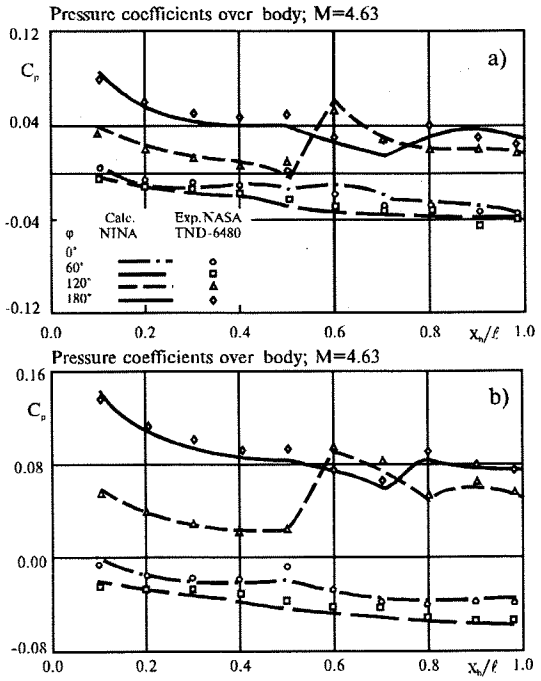

FIGURE 18

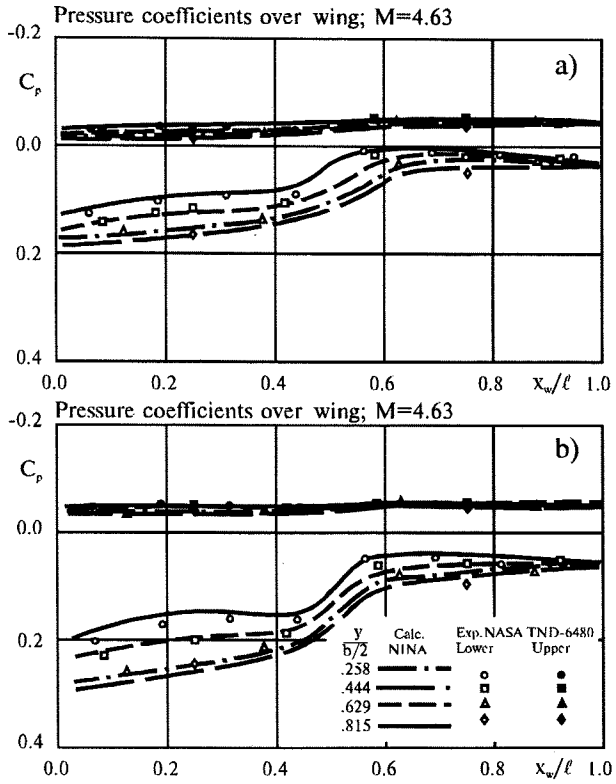

FIGURE 19

The previously mentioned numerical method based on theory[1] permits us to obtain the pressure coefficients which are in reasonable agreement with experimental data through the test Mach number range.

Body+cruciform delta wing+various horizontal canards

Static longitudinal stability and control characteristics of a configuration with cruciform delta wings and various horizontal canards have been investigated by this method at Mach numbers from 2. to 4.63 through an angle of attack range from 0 to 30°.

The results have been compared with experimental data obtained in the Langley Unitary Plan Wind tunnel[14].

A drawing of the model is shown in fig. 20. Figure 21 presents the aerodynamic coefficients for the model with canards C1 and C3 at M_∞=4.63. Fig. 21 is typical for whole range of Mach numbers. A comparison of the numerical results with experimental data indicates little disagreement between numerical and experimental data. Effect of canards C1 and C2 on coefficients C_a, C_n, C_d, C_l and L/D is very close to the C1 one. Moment coefficients for C1 and C2 differ significantly from the C3 one. This is why the results for C1 and C2 are shown for moment coefficients only.

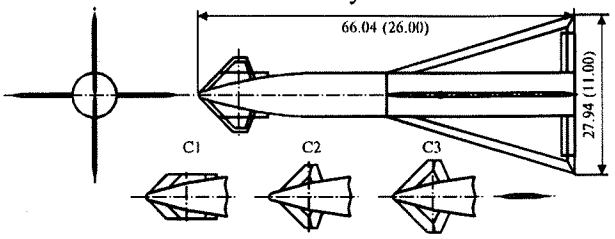

FIGURE 20

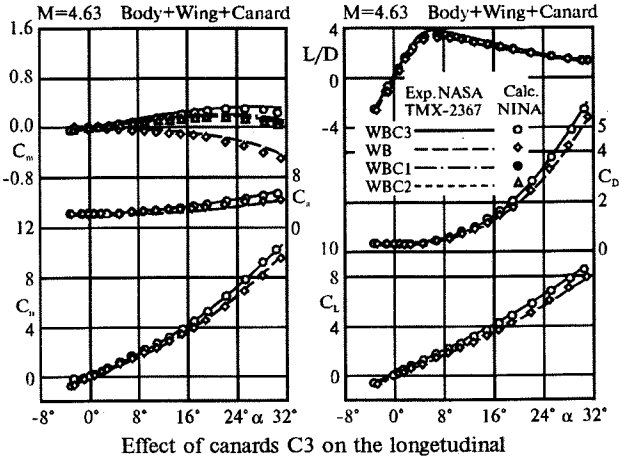

Effect of canards C3 on the longetudinal

FIGURE 21

Cruciform configuration of body+wing+canard

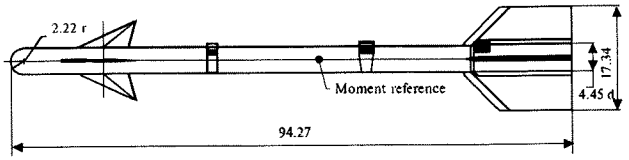

FIGURE 22

The aerodynamics of a cruciform configuration with triangular canard controls and trapezoidal wing have been investigated using this method. A drawing of the model is presented as Fig. 22. The cylindrical model fuselage is incorporated a hemisphere nose. Sychev's theory is applicable to the bodies which surface inclination is small. But around blunt nose, where surface inclination is up to 90° we have to use some spatial methods to determine the flow parameters. Pressure distribution over blunt nose have been obtained by modified Newton's method. Calculations started from the cross-section X=0.9 r. The typical results obtained during this investigation are shown for M =2.96 by fig.23 – roll angle φ=0 (scheme +), and fig. 24 – roll angle φ=45° (scheme X).

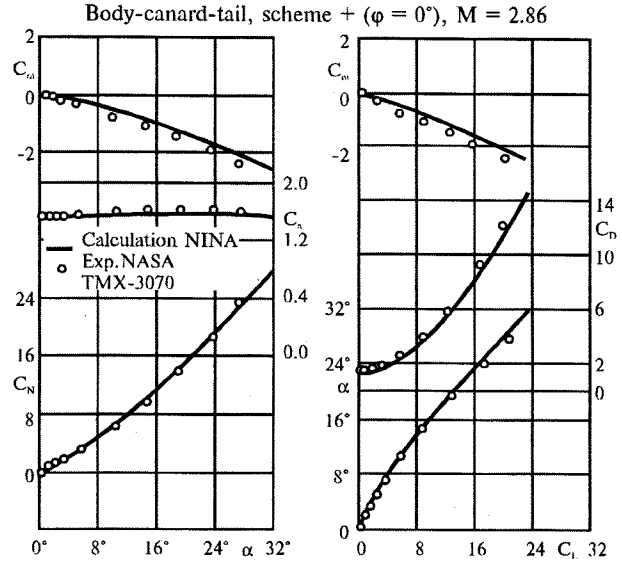

FIGURE 23

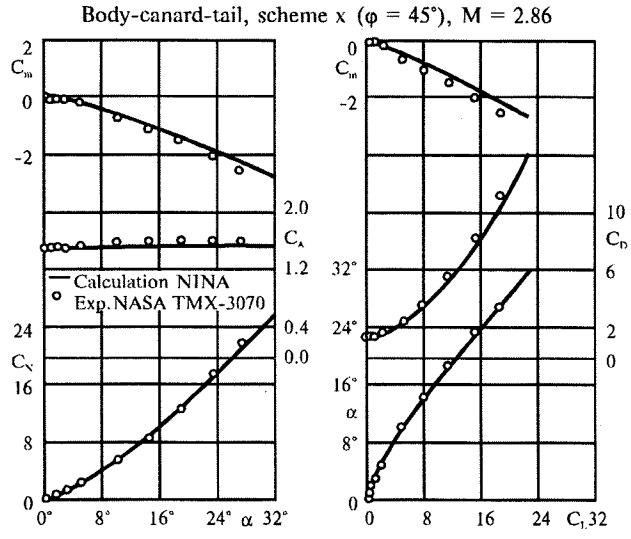

FIGURE 24

This investigation indicates that the method under consideration is effective for the configurations with canards which produce a pitching moment.

Conclusions

Theoretical consideration of the possibilities of the numerical method, based on Sychev's theory[1] and Godunov's method, shows that this method has a wide applicability region (fig. 5). It can be applied to the various airframes.

Numerical investigations and the comparison of its results with experimental data for a variety of body, body-wing, body-wing-canard configurations indicate that this method can be reliably applied to such practical configurations.

References

1. Sychev V.V. Three-Dimensional Hypersonic Gas Flow Past Slender Bodies at High Angles of Attack. J.Appl.Amth.Mech., v.24, No.2, 1960.
2. Hemsch M.J. Engineering analysis of slender-body aerodynamics using Sychev similarity parameters. J. Aircraft, 1988, V.25, No. 7, p.825-831.
3. Barnwell R.W. Extension of hypersonic high-incidence, slenderbody similarity. AIAA J. 1987, V. 25, No. 11, p. 1519-1522.
4. Hayes W.D. On Hypersonic Similitude. Quart.Appl.Math., v.5, No.1, April 1947.
5. Godunov S.K., Zabrodin A.V., Ivanov M.J., Krajko A.N.,Prokopov G.P. Numerical solution of multidimensional gasdynamics problems. Moscow, "Nauka", 1976.
6. KrajkoA.N., Makarov V.E., Tillajeva N.I. On numerical construction of shock-wave fronts. J. of Num. Math. and Math. Phys., V. 20, No. 3, 1980.
7. Lunev V.V. Hypersonic aerodynamics. Moscow, "Mashinostroenie", 1975.
8. Melnikov D.A. Supersonic flow around flat delta wing. "Izv. AN SSSR, Mech. i Mashinostroenie", 1962, No. 6, p.33-39.
9. Bazjin A.P. Calculation of ideal gas flow over flat delta wings at high angles of attack. "Trudy TsAGI", 1966, V. 1034, p. 3-28.
10. Bogatko V.I., Grib A.A., Kolton G.A. Hypersonik gas flow over slender wing of variable form. "Izv AN SSSR, MJG", 1979, No. 4, p. 94-101.
11. Landrum E.J. Wind-tunnel pressure data at Mach numbers from 1.6 to 4.63 for a series of bodies of revolution at angles of attack from -4 to 60 . NASA TM X-3558,1977.
12. Sprearmen M.L., Trescot C.D. Effect of wing planform on the static aerodynamics of a cruciform wing-body missile for Mach numbers up to 4.63. NASA TM X-1839, 1969.
13. Jernell L.S. Comparison of theoretical and experimental pressure distributions over a wing-body model at high supersonic speeds. NASA TN D-6480, 1971.
14. Trescot C.D. Longetudinal aerodynamic characteristics at Mach 1.50 to 4.63 of a missile model emloying various canards and trailing-edge flap control. NASA TM X-2367,1971.
15. Graves E.B., Fournier R.H. Stability and control characteristics at Mach numbers from 0.20 to 4.63 of a cruciform air-to-air missile with triangular canard controls and a trapezoidal wing. NASA TM X-3070, 1974.